

This is a repository copy of *A semi-parametric estimation method for quantile coherence with an application to bivariate financial time series clustering*.

White Rose Research Online URL for this paper:

<https://eprints.whiterose.ac.uk/224774/>

Version: Accepted Version

Article:

Jimenez Varon, Cristian Felipe orcid.org/0000-0001-7471-3845, Sun, Ying and Li, Ta Hsin (2024) A semi-parametric estimation method for quantile coherence with an application to bivariate financial time series clustering. *Econometrics and Statistics*. ISSN 2452-3062

Reuse

This article is distributed under the terms of the Creative Commons Attribution (CC BY) licence. This licence allows you to distribute, remix, tweak, and build upon the work, even commercially, as long as you credit the authors for the original work. More information and the full terms of the licence here:

<https://creativecommons.org/licenses/>

Takedown

If you consider content in White Rose Research Online to be in breach of UK law, please notify us by emailing eprints@whiterose.ac.uk including the URL of the record and the reason for the withdrawal request.



Contents lists available at ScienceDirect

Econometrics and Statistics

journal homepage: www.elsevier.com/locate/ecosta

A semi-parametric estimation method for quantile coherence with an application to bivariate financial time series clustering

Cristian F. Jiménez-Varón^{a,b,*}, Ying Sun^c, Ta-Hsin Li^d^a Department of Mathematics, University of York, Heslington, York YO10 5DD, United Kingdom^b Department of Physics and Mathematics, Universidad Autónoma de Manizales, Manizales 170002, Colombia^c CEMSE Division, Statistics Program, King Abdullah University of Science and Technology, Thuwal, 23955-6900, Saudi Arabia^d IBM Watson Research Center, New York, United States

ARTICLE INFO

Article history:

Received 29 February 2024

Revised 7 November 2024

Accepted 11 November 2024

Available online xxx

Keywords:

Clustering

Financial stocks

Financial time series

Quantile coherence

Quantile spectral analysis

VAR approximation

ABSTRACT

In multivariate time series analysis, spectral coherence traditionally measures linear dependencies between time series across different frequencies but often fails to capture nonlinear dependencies. In contrast, quantile coherence detects these nonlinear relationships across various quantile levels using trigonometric quantile regression. A new semi-parametric technique for estimating quantile coherence is introduced, combining the parametric spectrum of a vector autoregressive (VAR) model with nonparametric smoothing across quantiles. For each quantile level, the quantile autocovariance function (QACF) is obtained by applying the Fourier inverse transform to quantile periodograms. The multivariate Durbin-Levinson algorithm is then used to estimate the VAR parameters, which are subsequently applied to derive the quantile coherence estimate. A nonparametric smoother is applied across quantiles to enhance the initial estimate. Numerical results demonstrate that this method outperforms traditional nonparametric approaches. Moreover, clustering bivariate time series based on quantile coherence shows advantages over using ordinary VAR coherence. For instance, when applied to financial stocks, quantile coherence identifies clusters with a more informative structure, providing insights into diversified investment portfolios, which could help investors make better decisions.

© 2024 The Authors. Published by Elsevier B.V. on behalf of EcoSta Econometrics and Statistics.

This is an open access article under the CC BY license (<http://creativecommons.org/licenses/by/4.0/>)

1. Introduction

For univariate time series, motivated by the least-squares interpretation of the ordinary periodogram (OP), Li (2012) proposed the quantile periodogram (QPER) based on trigonometric quantile regression. The QPER, like the ordinary periodogram, has an asymptotic exponential distribution where the mean function, known as the quantile spectrum, is a scaled version of the ordinary spectrum of the level-crossing process. In Li (2012) the QPER is shown to be resistant to nonlinear

* Corresponding author.

E-mail address: cristian.jimenezvaron@york.ac.uk (C.F. Jiménez-Varón).

<https://doi.org/10.1016/j.ecosta.2024.11.002>

2452-3062/© 2024 The Authors. Published by Elsevier B.V. on behalf of EcoSta Econometrics and Statistics. This is an open access article under the CC BY license (<http://creativecommons.org/licenses/by/4.0/>)

data distortion in the sense that any nonlinear memoryless transformation only affects the scaling constant in the asymptotic distribution in the given quantile. Wise et al. (1977) shows that OP is not resistant to such nonlinear data transformations as the power spectrum is distorted.

The QPER can be extended to multivariate time series, and in particular, the quantile coherence quantifies the nonlinear dependency across time series by defining coherence as a function of quantile levels as well as frequencies. The quantile coherence has an advantage over its ordinary coherence counterpart as its asymptotic distribution relies on the level-crossing cross-spectrum, which, like QPER, is resistant to nonlinear data distortion due to the robustness of quantile regression (Li, 2013). Even though quantile coherence is a more effective tool, how to estimate it remains an interesting question.

Periodogram smoothing is the first that comes to mind. In time series analysis, many methods exist to smooth periodograms for univariate time series. For instance, Shumway and Stoffer (2017) presented several nonparametric periodogram smoothing approaches that can be used across frequencies, such as moving-average smoothing. The optimally smoothed spline (OSS) estimator by Wahba (1980) selects the smoothing parameter by minimizing the expected integrated mean square error. Some other common spectral estimations are based on the likelihood. For instance, Capon (1983) used a high-resolution estimation method, known as the maximum-likelihood method (MLM). MLM filters the time series to produce the minimum-variance unbiased estimator of the spectrum. For bivariate time series data, Pawitan and O'Sullivan (1994) estimated the spectrum by means of the penalized Whittle likelihood. In terms of parametric estimators, Burg (1975) presented the maximum entropy type of estimators, which in the univariate case results in the autoregressive (AR) spectral approximation. Dette et al. (2015) demonstrated that a window smoother of the quantile periodogram may consistently estimate the quantile spectrum across frequencies. Chen et al. (2021) employed a semi-parametric estimation of the quantile spectrum by using the approximation capability of the AR model. A nonparametric smoother is proposed to smooth both quantile levels and AR coefficients in the partial autocorrelation function (PACF) domain. Baruník and Kley (2019) introduced a nonparametric quantile coherence estimator based on the level-crossing process; in addition, to achieve consistency of the estimator, they proposed smoothing the proposed copula cross-periodogram across frequencies based on the results for the univariate case, initially introduced by Kley et al. (2016) (Proposition 3.4).

An alternative technique is introduced for estimating quantile coherence, employing a semi-parametric approach that integrates the parametric spectrum of a vector autoregressive (VAR) model with nonparametric smoothing across quantile levels. The estimator relies on the assumption that the true quantile coherence, viewed as a bivariate function of frequencies and quantiles, demonstrates smoothness across quantile levels.

A key distinction between the presented approach and the method introduced by Baruník and Kley (2019) lies in the nature of the estimated quantile coherence. The estimator considers both frequencies and quantile levels as bivariate inputs, covering a range of quantile values within the interval (0,1) rather than a single fixed level. In contrast, the estimator introduced by Baruník and Kley (2019) applies kernel smoothing across frequencies, necessitating careful selection of both a bandwidth parameter and kernel type to ensure consistency. In contrast, the semi-parametric approach utilizes the VAR representation of the quantile spectra at each quantile level. The order of the VAR can be determined using an automatic selection method such as AIC, which simplifies the process compared to optimal bandwidth selection.

The concept of employing a parametric autoregressive (AR) model for spectrum estimation has been advocated by researchers such as Akaike (1969); Parzen (1983); Newton and Pagano (1981). Additionally, the maximum entropy framework has been used to characterize autoregressive spectral densities as models for the spectral density of a stationary time series (Burg, 1975; Choi, 1993; Parzen, 1982). In the univariate case, the spectral density function of a stationary process can be approximated by the spectral density function of an autoregressive (AR) process Shumway and Stoffer (2017) (Property 4.7, see Appendix C.6 for more details). This property also holds for other time series representations, such as the moving average (MA) process or the autoregressive moving average (ARMA) process. For multivariate time series, Wiener and Masani (1957) (Theorem 7.13) demonstrates that a given non-negative Hermitian matrix-valued function can be factorized into the product of two functions defined over the complex plane. Wiener and Masani (1958) (Section 2) introduces the vector autoregressive (VAR) as a means of determining the matrix coefficients of the generating functions in the factorization representation. Offering a theoretical justification, such as consistency, is challenging due to the lack of a closed-form solution and uniform error bounds for the quantile regression coefficients. Although we have not thoroughly analyzed the theoretical properties of our proposed estimator, empirical studies suggest that it performs well in practical applications. We recognize that further theoretical exploration is an important direction for future research.

The proposed parametric approach for estimating quantile coherence follows a three-step process. First, the quantile autocovariance function (QACF) is derived from the quantile periodograms at fixed quantile levels. Next, the vector autoregressive (VAR) parameters are computed based on the QACF using the Durbin-Levinson algorithm, with the order of the VAR approximation for all quantile levels automatically selected via the AIC criterion (Akaike, 1974). This is followed by obtaining the initial quantile coherence estimate using the VAR models. A nonparametric smoother is then applied to refine this initial estimate across quantile levels for each frequency. Assuming that the degree of smoothness across quantiles remains relatively stable across frequencies, a cross-validation criterion is introduced to select a common tuning parameter for all frequencies. Empirical performance of the estimation method is evaluated through a simulation study.

Spectral features, including spectral coherence, have been used as input for many applications in time series classification and clustering (Euán et al., 2019; Chen et al., 2021). Maadooliat et al. (2018) applied their proposed spectral density estimation methods for brain signal clustering. Euán et al. (2019) developed a coherence-based hierarchical clustering method with application to brain connectivity. The quantile frequency analysis (QFA) (see, e.g., Li, 2020; 2021) uses a two-

dimensional function of the quantile spectral estimate by varying the quantile level as well as the trigonometric frequency parameter. The QFA method has been used in two ways in classification. The first method treats quantile periodograms as images that can be directly fed into a deep-learning image classifier like convolutional neural networks (CNN). The second method employs dimension-reduction techniques and feeds the resulting features into a general-purpose classifier such as the support vector machine (Hastie et al., 2017). Chen et al. (2021) used the former approach to classify earthquake waves. Li (2020) used the latter approach to classify real-world ultrasound signals for nondestructive evaluation of the structural integrity of aircraft panels.

Financial time series clustering was examined by Bishnoi and Ravishanar (2018) using a quantile periodogram approach with stock price data from various sectors. In the realm of risk analysis, Baruník and Nevrla (2022) introduced the concept of quantile spectral beta (QSB) to represent risk, leveraging the quantile cross-spectral densities proposed by Baruník and Kley (2019) to capture tail and spectral risks at a specific quantile level.

The application section explores clustering of 52 stocks based on their quantile coherence with the S&P 500 (SPX) index across specific quantile regions. For each stock, daily log returns are paired with corresponding S&P 500 closing prices to form a 2D vector time series, from which quantile coherence is computed. This quantile coherence, which accounts for both frequencies and quantile levels, serves as input for hierarchical clustering. To assess the clusters formed using quantile coherence, they are compared to clusters generated through the standard coherence method. Additionally, the clusters are evaluated against those derived from the time-domain approach, which employs the beta coefficient in the Capital Asset Pricing Model (CAPM). Results indicate that quantile coherence provides supplementary, valuable insights and generally yields more meaningful clusters.

The remainder of the paper is organized as follows: Section 2 introduces the concept of quantile coherence and the proposed estimation procedure. Section 3 presents the simulation study, while Section 4 details the application to financial time series clustering. Conclusions and a discussion are provided in Section 5.

2. Methodology

This section begins with an introduction to the quantile spectrum, quantile periodogram, and quantile coherence in Section 2.1. Section 2.2 discusses the VAR spectral model and its estimation. The VAR representation of the estimated quantile spectral matrix is covered in Section 2.3. Finally, Section 2.4 presents the proposed smoothing procedure for the VAR spectrum.

2.1. Quantile spectrum and quantile coherence

Assume $Y_{t,j}$ ($j = 1, \dots, k$) are k jointly stationary random processes. Let $F_j(u)$ denote the CDF of $Y_{t,j}$, which is a continuous function with the derivative $\dot{F}_j(u) > 0$. Let $\lambda_{j,\alpha}$ denote the α quantile of $Y_{t,j}$ for $\alpha \in (0, 1)$. Finally, let $\gamma_{\tau,j,j'}(\alpha) := \mathbb{P}\{(Y_{t+\tau,j} - \lambda_{j,\alpha})(Y_{t,j'} - \lambda_{j',\alpha}) < 0\}$ denote the lag- τ level-crossing rate of $Y_{t,j}$ and $Y_{t,j'}$. Then, according to Li (2012, 2013), the quantile cross-spectrum is defined as

$$s_{j,j'}(\omega, \alpha) = \eta_{j,\alpha} \eta_{j',\alpha} f_{j,j'}(\omega, \alpha),$$

where

$$f_{j,j'}(\omega, \alpha) = \sum_{\tau=-\infty}^{\infty} \left\{ 1 - \frac{1}{2\alpha(1-\alpha)} \gamma_{\tau,j,j'}(\alpha) \right\} \exp(i2\pi\omega\tau), \quad i = \sqrt{-1},$$

is called the level-crossing spectrum, and the scaling constants are defined as $\eta_{j,\alpha} := \sqrt{\alpha(1-\alpha)}/\dot{F}_j(\lambda_{j,\alpha})$ and $\eta_{j',\alpha} := \sqrt{\alpha(1-\alpha)}/\dot{F}_{j'}(\lambda_{j',\alpha})$.

Given the observations $Y_{t,j}$ ($t = 1, \dots, n$) and quantile level $\alpha \in (0, 1)$, consider the following quantile regression problem:

$$\widehat{\beta}_{n,j}(\omega, \alpha) := \arg_{\lambda_{j,\alpha} \in \mathbb{R}, \beta_j \in \mathbb{R}^2} \min \sum_{t=1}^n \rho_{\alpha}(Y_{t,j} - \lambda_{j,\alpha} - \mathbf{x}_t^{\top}(\omega) \beta_j), \quad (1)$$

where $\rho_{\alpha}(u) := u(\alpha - \mathbb{I}(u < 0))$ and $\mathbf{x}_t(\omega) := [\cos(2\pi\omega t), \sin(2\pi\omega t)]^{\top}$ for $\omega \in (0, 1/2)$.

Let $\widehat{\beta}_{n,j}(\omega, \alpha) := [\widehat{A}_{n,j}(\omega, \alpha), \widehat{B}_{n,j}(\omega, \alpha)]^{\top}$ denote the quantile regression solution given by Eq. (1). Then, the quantile cross-periodogram between $Y_{t,j}$ and $Y_{t,j'}$ is defined as

$$q_{j,j',n}(\omega, \alpha) = n z_j(\omega, \alpha) z_{j'}^*(\omega, \alpha), \quad j, j' = 1, \dots, k, \quad (2)$$

where $z_j(\omega, \alpha) := \frac{1}{2} \sqrt{n} \{\widehat{A}_{n,j}(\omega, \alpha) - i \widehat{B}_{n,j}(\omega, \alpha)\}$ and $*$ denotes the complex conjugate transpose. Notice that when $j = j'$ in Eq. (2), it becomes the quantile periodogram of the first kind as in Li (2012). In addition, with $\alpha = 0.5$ it is the Laplace periodogram by Li (2008) as a special case. It's important to note that the ordinary periodogram matrix, like the quantile periodogram matrix $(\mathbf{Q}(\omega_l, \alpha_m))$, can be obtained by substituting the quantile regression cost function with the least squares cost function and limiting ω to the Fourier frequencies.

Li (2013) provided the asymptotic properties of the quantile cross-spectrum for the multivariate time series problem. A connection between the quantile periodogram/cross-periodogram and the quantile spectra/cross-spectra was established in Li (2013) (Theorem 11.3), which states that under suitable conditions, the quantile periodogram matrix $\mathbf{Q}_n(\omega, \alpha) := [q_{j,j',n}(\omega, \alpha)]$ is asymptotically distributed as $\boldsymbol{\zeta}\boldsymbol{\zeta}^*$, where $\boldsymbol{\zeta} \sim \mathcal{N}_c(\mathbf{0}, \mathbf{S}(\omega, \alpha))$, with $\mathbf{S}(\omega, \alpha) := [s_{j,j'}(\omega, \alpha)]$.

The (squared) quantile coherence between $Y_{t,j}$ and $Y_{t,j'}$ is defined as

$$c_{j,j'}(\omega, \alpha) = \frac{|s_{j,j'}(\omega, \alpha)|^2}{s_{j,j}(\omega, \alpha)s_{j',j'}(\omega, \alpha)}. \quad (3)$$

It takes values between 0 and 1.

2.2. VAR Spectral Model

The VAR spectral model of order p takes the form

$$\mathbf{S}_{\text{VAR}}(\omega) = \mathbf{U}_p^{-1}(\omega) \mathbf{V}_p (\mathbf{U}_p^{-1}(\omega))^*, \quad (4)$$

where

$$\mathbf{U}_p(\omega) = \mathbb{I} - \sum_{r=1}^p \boldsymbol{\Phi}_r e^{-i2\pi r\omega}.$$

The model in (4), is the spectral matrix of the VAR process $\{\mathbf{Y}_t\}$ and \mathbf{V}_p denotes the corresponding residual covariance matrix. $\{\mathbf{Y}_t\}$ satisfies (Priestley, 1981)

$$\mathbf{Y}_t + \boldsymbol{\Phi}_1 \mathbf{Y}_{t-1} + \dots + \boldsymbol{\Phi}_p \mathbf{Y}_{t-p} = \boldsymbol{\epsilon}_t, \quad (5)$$

where \mathbf{Y}_t is a k -dimensional vector and $\boldsymbol{\Phi}_1, \dots, \boldsymbol{\Phi}_p$ are $k \times k$ matrices, and $\boldsymbol{\epsilon}_t$ is a multivariate zero mean white noise process. Each of the components of the vector $\boldsymbol{\epsilon}_t$ is a univariate white noise process, uncorrelated with each other at different time points but possibly cross-correlated at common time points.

Assuming stationarity on the VAR model, we can obtain the multivariate Yule-Walker equations by multiplying both sides of Eq. (5) by \mathbf{Y}_{t-h}^\top and taking expectations. Denote the covariance matrix for \mathbf{Y}_t of nonzero lag h by $\boldsymbol{\Gamma}(h)$, this gives,

$$\boldsymbol{\Gamma}(h) + \boldsymbol{\Phi}_1 \boldsymbol{\Gamma}(h-1) + \dots + \boldsymbol{\Phi}_p \boldsymbol{\Gamma}(h-p) = \mathbf{0},$$

In matrix form, this can be written as

$$-[\boldsymbol{\Gamma}(1), \boldsymbol{\Gamma}(2), \dots, \boldsymbol{\Gamma}(p)] = [\boldsymbol{\Phi}_1, \boldsymbol{\Phi}_2, \dots, \boldsymbol{\Phi}_p] \tilde{\boldsymbol{\Gamma}}, \quad (6)$$

where

$$\tilde{\boldsymbol{\Gamma}} = \begin{bmatrix} \boldsymbol{\Gamma}(0) & \boldsymbol{\Gamma}(1) & \dots & \boldsymbol{\Gamma}(p-1) \\ \boldsymbol{\Gamma}(1)^\top & \boldsymbol{\Gamma}(0) & \dots & \boldsymbol{\Gamma}(p-2) \\ \vdots & \vdots & \ddots & \vdots \\ \boldsymbol{\Gamma}(p-1)^\top & \boldsymbol{\Gamma}(p-2)^\top & \dots & \boldsymbol{\Gamma}(0) \end{bmatrix}.$$

The Yule-Walker equations in (6) must be solved for $\boldsymbol{\Phi}_r, r = 1, \dots, p$. A brute-force approach requires the inversion of $kp \times kp$ matrices. The multivariate version of the Durbin-Levinson algorithm (see Appendix A.1) can be used to speed up the computation. From the VAR spectral model of order p in (4), the ordinary VAR coherence can be computed by,

$$c_{j,j'}(\omega) = \frac{|s_{j,j'}(\omega)|^2}{s_{j,j}(\omega)s_{j',j'}(\omega)}.$$

2.3. VAR estimator of quantile coherence

The ordinary periodogram matrix $\mathbf{I}_n(\omega)$ for any frequency $\omega \in [0, 1)$ is defined by

$$\mathbf{I}_n(\omega) = \mathbf{J}(\omega)\mathbf{J}^*(\omega),$$

where $\mathbf{J}(\omega) = n^{-1/2} \sum_{t=1}^n (\mathbf{Y}_t - \bar{\mathbf{Y}}) e^{-i2\pi\omega t}$. It is easy to show that

$$\mathbf{I}_n(\omega) = \sum_{|h|<n} \hat{\boldsymbol{\Gamma}}(h) e^{-ih2\pi\omega}, \quad (7)$$

where $\hat{\boldsymbol{\Gamma}}(h) = n^{-1} \sum_{t=1}^{n-h} (\mathbf{Y}_{t+h} - \bar{\mathbf{Y}})(\mathbf{Y}_t - \bar{\mathbf{Y}})^\top, h \geq 0$, and $\hat{\boldsymbol{\Gamma}}(h) = \hat{\boldsymbol{\Gamma}}^\top(-h), h < 0$. By the $2n$ -point inverse discrete Fourier transform, the sample autocovariance function (ACF) $\hat{\boldsymbol{\Gamma}}(h)$ can be recovered from the periodogram, as follows,

$$\hat{\boldsymbol{\Gamma}}(h) = (2n)^{-1} \sum_{l=0}^{2n-1} \mathbf{I}_n(\omega_l) e^{ih2\pi\omega_l}, \quad (8)$$

where $\omega_l = l/2n$. (See the [Appendix A.2](#) for the mathematical proof). This relationship motivates the presented VAR spectral estimator.

To estimate the quantile coherence, the approach utilizes a parametric Vector Autoregressive (VAR) spectrum of order p to approximate the quantile spectral matrix $\mathbf{S}(\omega, \alpha_m)$ for a given set of equally spaced quantile levels $\alpha_m, m = 1, \dots, n_q$ within the interval $(0, 1)$. The raw extended quantile periodogram matrix $\mathbf{Q}_n(\omega_l, \alpha_m)$ is derived from the time series, where $\omega_l = \frac{l}{2n}$, representing the quantile counterpart of the ordinary periodogram matrix as defined in [Equation \(7\)](#). Fourier frequencies are computed over the first half and extended symmetrically. By applying the $2n$ -point inverse Fourier transform to $\mathbf{Q}(\omega_l, \alpha_m)$, the Quantile Autocovariance Function (QACF) is obtained, following a similar approach to that described in [Equation \(8\)](#). The QACF is then computed as follows:

$$\hat{\Gamma}_h(\alpha_m) = (2n)^{-1} \sum_{l=0}^{2n-1} \mathbf{Q}_n(\omega_l, \alpha_m) e^{i2\pi\omega_l h}, \quad h = 0, 1, \dots, n-1. \quad (9)$$

We use the multivariate Durbin-Levinson algorithm to solve the multivariate Yule-Walker equations in [\(6\)](#) formed by $\hat{\Gamma}_h(\alpha_m)$ in [Eq. \(9\)](#) for each fixed α_m . This algorithm produces the VAR coefficients $\hat{\Phi}_1(\alpha_m), \dots, \hat{\Phi}_p(\alpha_m)$ and the residual covariance matrix $\hat{\mathbf{V}}_p(\alpha_m)$ (see [Appendix A.1](#)). The quantile VAR spectrum of order p can be expressed as

$$\hat{\mathbf{S}}_{\text{QVAR}}(\omega, \alpha_m) = \hat{\mathbf{U}}_p^{-1}(\omega, \alpha_m) \hat{\mathbf{V}}_p(\alpha_m) (\hat{\mathbf{U}}_p^{-1}(\omega, \alpha_m))^*, \quad (10)$$

where,

$$\hat{\mathbf{U}}_p(\omega, \alpha_m) = \mathbb{I} - \sum_{r=1}^p \hat{\Phi}_r(\alpha_m) e^{-i2\pi r\omega}.$$

We propose to choose the order of the VAR model by minimizing the Akaike information criterion (AIC) ([Akaike, 1974](#)), i.e.,

$$\hat{p} = \arg \min_{p \in \{0, 1, \dots, p_{\max}\}} \left\{ \frac{1}{n_q} \sum_{m=1}^{n_q} n \log |\hat{\mathbf{V}}_p(\alpha_m)| + 2k^2 p \right\},$$

where n is the length of the time series, k is the number of time series ([Lütkepohl, 2005](#)). Some other order selection criterion includes the Bayesian information criterion (BIC) by [Schwarz \(1978\)](#) and the corrected AIC (AIC_c) by [Hurvich and Tsai \(1989\)](#).

Let the j, j' -th entry of $\hat{\mathbf{S}}(\omega, \alpha_m)$ in [\(10\)](#) be denoted by $\hat{s}_{j,j'}(\omega, \alpha_m)$. Then, the preliminary parametric estimate of the quantile coherence $\hat{c}_{j,j'}(\omega, \alpha_m)$ in [\(1\)](#) is defined as

$$\hat{c}_{j,j'}(\omega, \alpha_m) = \frac{|\hat{s}_{j,j'}(\omega, \alpha_m)|^2}{\hat{s}_{j,j}(\omega, \alpha_m) \hat{s}_{j',j'}(\omega, \alpha_m)}. \quad (11)$$

2.4. Smoothing spline procedure

Based on the assumption that true quantile coherence displays smoothness across quantiles, an improvement is proposed for the parametric estimator of quantile coherence in [Eq. \(11\)](#). This approach involves smoothing the estimates across quantile levels using smoothing splines at each frequency, with a shared tuning parameter.

Let the preliminary parametric quantile coherence estimate in [\(11\)](#) be evaluated at n_q quantile levels $\{\alpha_m\}_{m=1, \dots, n_q}$. For each frequency ω_l , a one-dimensional sequence $\{\hat{c}_{j,j'}(\omega_l, \alpha_m) : m = 1, \dots, n_q\}$ is obtained, which is then smoothed using smoothing splines. A straightforward method applies a standard smoothing spline procedure, such as the `smooth.spline` function in [R](#), independently to each of these sequences, with smoothing parameters selected by the standard leave-one-

out cross-validation technique. However, two potential issues arise with this method. First, using different smoothing parameters for different frequencies may introduce undesirable discontinuities across frequencies. Additionally, the standard leave-one-out cross-validation criterion can be ineffective in addressing positive correlations ([Altman, 1990; Wang, 1998](#)), as observed in the preliminary coherence estimate across quantile levels. To mitigate these issues, a smoothing procedure is proposed that employs a common λ for all frequencies, allowing the final quantile coherence estimate to be expressed as

$$\tilde{c}(\omega_l, \cdot) := \arg \min_{c(\omega_l, \cdot)} \left\{ \sum_{m=1}^{n_q} [\hat{c}(\omega_l, \alpha_m) - c(\omega_l, \alpha_m)]^2 + \lambda \int_0^1 \left[\frac{\partial^2 c(\omega_l, \alpha)}{\partial \alpha^2} \right]^2 d\alpha \right\}, \quad l = 1, \dots, n_f. \quad (12)$$

To select the common smoothing parameter λ , a special \mathcal{K} -fold cross-validation procedure is proposed. At each frequency ω_l , the sequence $\{\hat{c}_{j,j'}(\omega_l, \alpha_m) : m = 1, \dots, n_q\}$ is randomly split into \mathcal{K} (approximately) equal-size groups. For each $\kappa = 1, \dots, \mathcal{K}$, one of the groups is reserved for testing, while the remaining $\mathcal{K} - 1$ groups are used for training. Unlike a typical \mathcal{K} -fold cross-validation procedure, the mean value of the coherence estimates in the training set, denoted as $\bar{c}_{\text{pred}, \kappa}(\omega_l)$,

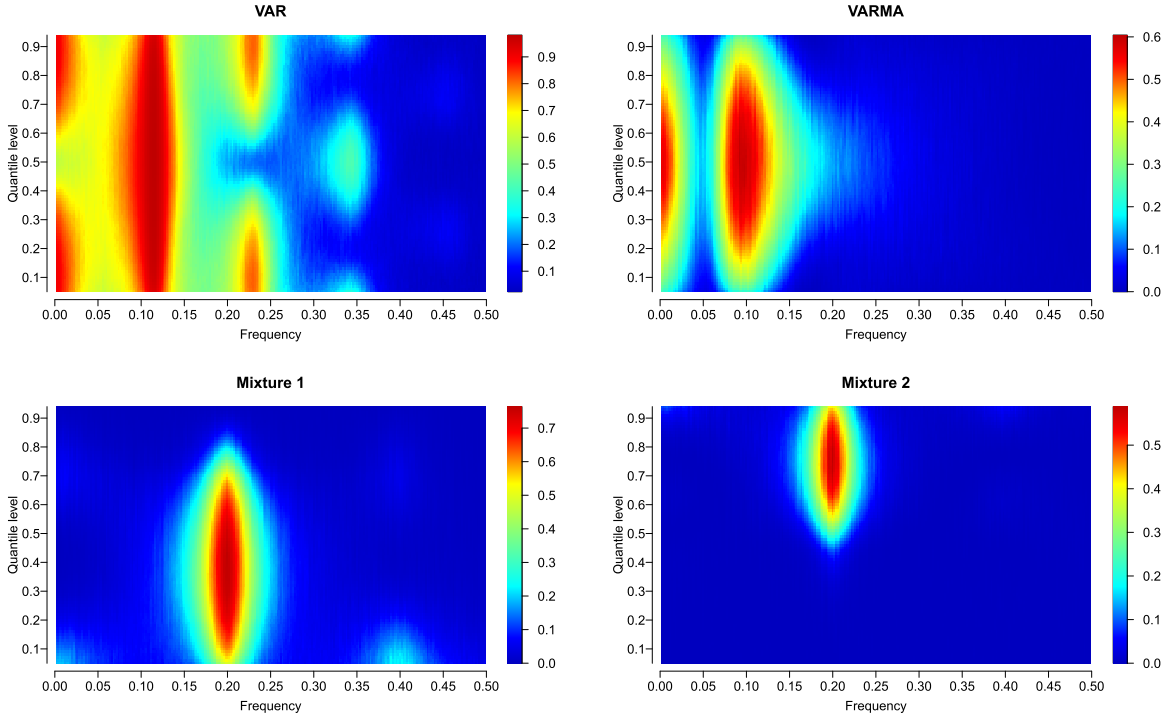


Fig. 1. The true quantile coherence of the 4 considered models with $n = 500$ for both VAR and VARMA models (top), Mixture 1, and Mixture 2 (bottom).

is utilized to predict the mean value of the coherence estimates in the testing set, denoted as $\bar{c}_{\text{test},\kappa}(\omega_l)$. The smoothing parameter λ is chosen as the minimizer of the following CV criterion:

$$CV(\lambda) = \sum_{\kappa=1}^{\mathcal{K}} \left\{ \sum_{l=1}^{n_f} [\bar{c}_{\text{pred},\kappa}(\omega_l) - \bar{c}_{\text{test},\kappa}(\omega_l)]^2 \right\}. \quad (13)$$

The proposed CV criterion in (13) uses mean value prediction to address the correlation of the sequences across quantile levels. The standard \mathcal{K} -fold cross-validation criterion predicts individual values in the test set. Due to the positive correlation of the residuals, the resulting tuning parameter tends to be very small for all frequencies, leading to minimal smoothing.

It is important to clarify that employing a common λ does not completely eliminate the discontinuity issue. However, it helps mitigate the problem by reducing the statistical variability that arises from using different λ values.

3. Simulation Study

In this section, the results of a simulation study are presented, comparing the proposed method with several alternatives in estimating the quantile coherence of simulated time series. Additionally, the results of clustering bivariate time series based on both quantile coherence and ordinary coherence are discussed.

3.1. Simulation setup

The models considered in this simulation setting are

1. VAR(2) model: $\mathbf{Z}_t = \mathbf{A}_1 \mathbf{Z}_{t-1} + \mathbf{A}_2 \mathbf{Z}_{t-2} + \mathbf{W}_t$, $\mathbf{W}_t \sim \mathcal{N}(\mathbf{0}, \Sigma)$,

$$\mathbf{A}_1 = \begin{bmatrix} 1.5 & -0.6 \\ 0.3 & 0.2 \end{bmatrix}, \mathbf{A}_2 = \begin{bmatrix} -0.5 & 0.3 \\ 0.7 & -0.2 \end{bmatrix}, \Sigma = \begin{bmatrix} 4 & 1 \\ 1 & 2 \end{bmatrix}.$$

2. VARMA(2,1) model: $\mathbf{Z}_t = \mathbf{A}_1 \mathbf{Z}_{t-1} + \mathbf{A}_2 \mathbf{Z}_{t-2} + \mathbf{W}_t - \mathbf{B}_1 \mathbf{W}_{t-1}$, $\mathbf{W}_t \sim \mathcal{N}(\mathbf{0}, \Sigma)$

$$\mathbf{A}_1 = \begin{bmatrix} 0.816 & -0.623 \\ -1.116 & 1.074 \end{bmatrix}, \mathbf{A}_2 = \begin{bmatrix} -0.643 & 0.592 \\ 0.615 & -0.133 \end{bmatrix},$$

$$\mathbf{B}_1 = \begin{bmatrix} 0 & -1.248 \\ -0.801 & 0 \end{bmatrix}, \Sigma = \begin{bmatrix} 4 & 2 \\ 2 & 5 \end{bmatrix}.$$

3. Mixture model highly coherent at lower quantiles: the vector time series, $\mathbf{Z}_t = (Z_{t,1}, Z_{t,2})^\top$ is a nonlinear mixture of three components given by

$$\begin{aligned}\xi_1 &:= \mathcal{W}_1(U_{t,1})U_{t,2} + (1 - \mathcal{W}_1(U_{t,1}))U_{t,1}, \\ \text{and,} \\ Z_{t,1} &:= \mathcal{W}_2(\xi_1)U_{t,3} + (1 - \mathcal{W}_2(\xi_1))\xi_1,\end{aligned}$$

where $U_{t,1}$, $U_{t,2}$, and $U_{t,3}$ are AR processes of mean zero and variance 1, satisfying

$$\begin{aligned}U_{t,1} &= 0.8U_{t-1,1} + w_{t,1}, \\ U_{t,2} &= -0.7U_{t-1,2} + w_{t,2}, \\ \text{and,} \\ U_{t,3} &= 0.55U_{t-1,1} - 0.81U_{t-2,3} + w_{t,3},\end{aligned}$$

where $w_{t,1}$, $w_{t,2}$, and $w_{t,3}$ are mutually independent Gaussian white noise. The mixing functions $\mathcal{W}_1(x)$ and $\mathcal{W}_2(x)$ are defined as follows

$$\begin{aligned}\mathcal{W}_1(x) &= \begin{cases} 0.1 & \text{if } x < -0.8 \\ 0.8 & \text{if } x > 0.8 \end{cases}, \\ \text{and,} \\ \mathcal{W}_2(x) &= \begin{cases} 0.5 & \text{if } x < -0.4 \\ 0 & \text{if } x > 0.4 \end{cases},\end{aligned}$$

where $\mathcal{W}_1(x)$ is linear between -0.8 and 0.8 ; $\mathcal{W}_2(x)$ is linear between -0.4 and 0.4 . The first component $U_{t,1}$ has a lowpass spectrum, $U_{t,2}$ has a highpass spectrum, and $U_{t,3}$ has a bandpass spectrum with a bandwidth of an AR(2) model with frequency at 0.20. The second component $Z_{t,2}$ of the vector time series \mathbf{Z}_t , is a delayed copy of $Z_{t,1}$ by 10 time units.

4. Mixture model highly coherent at higher quantiles: the vector time series $\mathbf{Z}_t = (Z_{t,1}, Z_{t,2})^\top$ is a nonlinear mixture of three components designed in a similar way as the previous mixture model. To obtain highly coherent higher quantiles, we just use another weighting function, $\mathcal{W}_2(x)$, which is defined as

$$\mathcal{W}_2(x) = \begin{cases} 0 & \text{if } x < -0.4 \\ 0.5 & \text{if } x > 0.4 \end{cases},$$

where $\mathcal{W}_2(x)$ is linear between -0.4 and 0.4 .

In the simulation study, two lengths of $n = 500$ and $n = 1000$ are considered for the VAR, VARMA, and nonlinear mixtures models. For each model and length, the average of 5000 raw quantile periodogram matrices is treated as the quantile spectral matrix, from which the true quantile coherence is derived. Figure 1 illustrates the true quantile coherence $\mathbf{C}(\omega, \alpha) := [c(\omega_l, \alpha_m)]$, $l = 1, \dots, n_f$, $m = 1, \dots, n_q$ for the VAR and VARMA models (top) and the mixture models (bottom) with $n = 500$. The quantile coherence is computed at 93 quantile levels, specifically 0.04, 0.05, \dots , 0.96. Extreme quantiles are excluded due to the potential for inappropriate behavior of the estimators.

3.2. Alternative Methods

In this study, the proposed estimation method for quantile coherence is compared to three alternative methods.

- (a) The nonparametric estimator proposed by Baruník and Kley (2019): quantile coherency is computed by utilizing the matrix of smoothed rank-based copula periodograms (CCR-periodograms) across frequencies for each fixed quantile level. The implementation of this estimator is available in the R package **Rquantspec** with the function **smoothedPG** (Kley, 2016). Specifically, when smoothing across frequencies, Baruník and Kley (2019) employs a kernel of order p , with the optimal bandwidth obtained approximately as $b_n \approx n^{-1/(2p+1)}$. In the current implementations, the default Epanechnikov kernel, which is a kernel of order $p = 2$ with an optimal bandwidth of approximately $b_n \approx n^{-1/5}$, is used. Three key distinctions between this approach and the method proposed in this study are noteworthy. First, the estimator by Baruník and Kley (2019) fixes the quantile level, while the proposed estimator considers the quantile level as a continuous variable within the interval $(0, 1)$. Second, the rank-based copula periodograms are utilized by Baruník and Kley (2019), whereas the proposed estimator is based on quantile periodograms obtained from trigonometric quantile regression. Lastly, the estimator by Baruník and Kley (2019) requires the selection of both kernel type and bandwidth for smoothing across frequencies and does not smooth across quantiles.
- (b) The 1D smoothing spline method: we smooth the raw quantile periodogram matrix using smoothing splines, first across frequencies for each fixed quantile level, and then across quantile levels for each fixed frequency; the quantile coherence is computed based on the resulting smoothed quantile periodogram matrix.

Table 1

This table presents the average root mean squared error (RMSE) of the quantile coherence estimates obtained from 200 simulation runs. The minimum value in each row for each of the five estimation methods is highlighted in bold. The standard error is also provided in parentheses.

Model	n	Semi-Param	Parametric	BK(2019)	S.spline	2D Kernel
VAR(2)	500	0.069 (0.010)	0.089 (0.008)	0.114 (0.004)	0.451 (0.017)	0.451 (0.017)
VAR(2)	1000	0.054 (0.006)	0.066 (0.006)	0.104 (0.003)	0.459 (0.014)	0.460 (0.014)
VARMA(2,1)	500	0.079 (0.011)	0.089 (0.010)	0.121 (0.009)	0.389 (0.069)	0.384 (0.058)
VARMA(2,1)	1000	0.059 (0.009)	0.065 (0.008)	0.118 (0.006)	0.383 (0.048)	0.380 (0.046)
Mixture 1	500	0.077 (0.010)	0.088 (0.009)	0.145 (0.013)	0.445 (0.077)	0.455 (0.062)
Mixture 1	1000	0.057 (0.007)	0.064 (0.006)	0.146 (0.010)	0.454 (0.067)	0.464 (0.046)
Mixture 2	500	0.065 (0.010)	0.067 (0.011)	0.078 (0.007)	0.490 (0.138)	0.531 (0.078)
Mixture 2	1000	0.045 (0.010)	0.047 (0.009)	0.075 (0.006)	0.466 (0.115)	0.490 (0.072)

- (c) The 2D kernel smoothing method: we apply 2D smoothing to the raw quantile periodograms as bivariate functions of frequency and quantile level and compute the quantile coherence from the resulting smoothed quantile periodogram matrix.

In addition, we also demonstrate the effectiveness of the smoothing across quantiles by comparing the final estimates in (12) which will be labeled as semi-parametric, with the preliminary estimates in (11) which will be labeled as parametric.

We use the following root mean squared error (RMSE) between the estimated quantile coherence and the true quantile coherence to measure the performance of an estimator:

$$D_{\text{RMSE}}\{\mathbf{C}, \tilde{\mathbf{C}}\} = \sqrt{\frac{1}{n_f n_q} \sum_{l=1}^{n_f} \sum_{m=1}^{n_q} [c(\omega_l, \alpha_m) - \tilde{c}(\omega_l, \alpha_m)]^2}.$$

The performance assessment of different cases is presented in Table 1, where the average root mean squared error (RMSE) is calculated based on 200 simulation runs. The estimation methods are labeled as follows: Semi-Param: Parametric estimator with smoothing across quantiles in (12). The smoothing parameter is selected using a five-fold cross-validation procedure, as described in Section 2.4. Parametric: VAR estimator of quantile coherence without smoothing in (11). BK (2019): Nonparametric estimator proposed by Baruník and Kley (2019). S.spline: 1D smoothing spline. 2D Kernel: 2D kernel smoothing. From the results in Table 1, it is evident that the proposed semi-parametric estimator, which incorporates smoothing across quantiles, consistently outperforms all other methods. The additional smoothing significantly improves the estimation of quantile coherence overall. Moreover, even without smoothing, the parametric estimator itself demonstrates superior performance compared to its competitors. Notably, it produces better simulation results than the nonparametric estimator proposed by Baruník and Kley (2019). Furthermore, we observe a decreasing trend in both the RMSE and standard error as the sample size (n) increases. This suggests that the accuracy of the estimators improves with larger sample sizes.

3.3. Clustering simulation

In this section, the problem of clustering bivariate ($k = 2$) time series based on the similarities of their quantile coherence is considered. A cluster is defined as a collection of bivariate time series that exhibit similar quantile coherence. The study does not extend to multivariate time series with dimensions greater than two ($k > 2$). Further research is needed to address both the estimation and clustering of higher-dimensional time series.

This method is compared with an alternative that employs the ordinary coherence derived from the VAR model of the bivariate time series. To derive the ordinary coherence, a VAR model is first fitted to a bivariate time series, and then the spectral matrix is computed using the parameters from the fitted VAR model. The ordinary coherence is defined by the VAR spectral matrix in a manner similar to (4). Through the simulation study, the potential benefit of quantile coherence for this problem is demonstrated compared to ordinary coherence.

The clustering simulation begins by considering the four models described in Section 3.1 as the true clusters. Two hundred bivariate time series are simulated from each of the four models, and their quantile coherence and ordinary coherence are computed. Both the quantile coherence and the ordinary coherence serve as dissimilarity measures for a hierarchical clustering procedure.

For each time series, a feature vector is created by collecting the quantile coherence $c_{1,2}(\omega_l, \alpha_m)$ for $l = 1, \dots, n_f$ and $m = 1, \dots, n_q$. The dissimilarity measure for a pair of time series is defined as the Euclidean distance between the corresponding quantile-coherence-based feature vectors. A similar method is employed to define the dissimilarity measure based on ordinary coherence.

Computing the dissimilarity measure for all pairs allows for the establishment of a pairwise distance matrix, which is used as input for hierarchical clustering. The optimal number of clusters is chosen based on the so-called ‘‘elbow rule’’ (Yuan and Yang, 2019), which utilizes the total within-cluster sum of squares (WSS) as a function of the number of clusters.

From the right panel of Figure 2, it can be clearly stated that the optimal number of clusters for the quantile coherence equals 4. In contrast, the left panel of Figure 2 indicates that the optimal number of clusters for the ordinary coherence

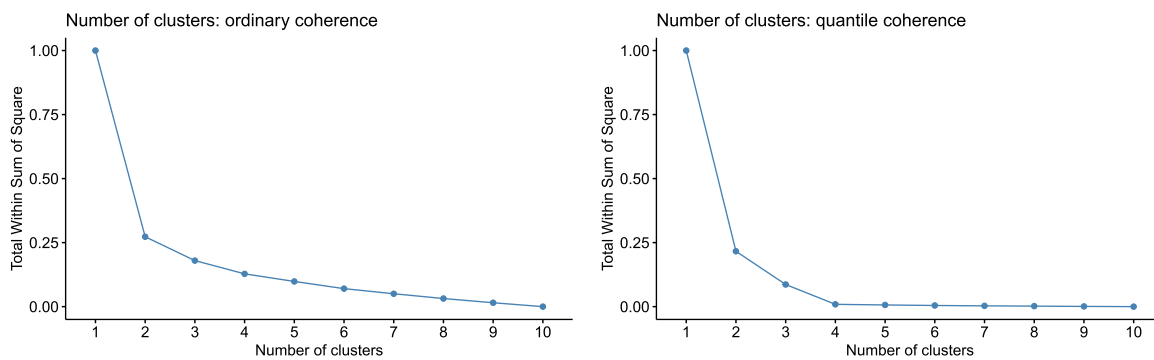


Fig. 2. The total within-cluster sum of squares (WSS) as a function of the number of clusters. Based on the ordinary coherence (left), based on the quantile coherence (right).

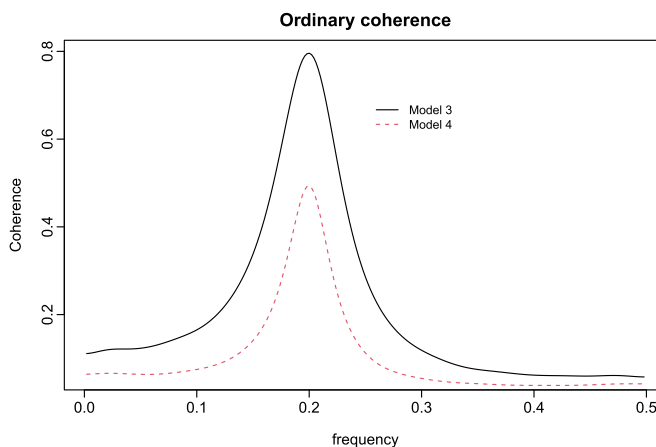


Fig. 3. The true ordinary coherence of the 2 mixture models (models 3 and 4), with $n = 500$.

lies between 3 and 4. In an initial exploratory exercise, it is assumed that the number of clusters identified by the quantile coherence, 4, is identical to the number of clusters formed from the ordinary coherence in order to evaluate the findings in terms of the allocation of members in each cluster.

Although the optimal number of clusters is the same in this case, the allocation results differ substantially. The ordinary coherence assigns the first cluster to the 200 bivariate series acquired by model 1, and similarly assigns the second cluster to model 2. Finally, the remaining 400 bivariate series generated by the mixture models are allocated to the third (196 members) and fourth (204 members) clusters. The third cluster predominantly contains simulated bivariate time series obtained from model 3, with only one case from model 4, while the fourth cluster primarily includes members obtained from model 4, along with a few cases from model 3.

In a second exercise, three clusters were chosen as the optimal number based on the ordinary coherence. The new results indicate that, as in the previous example, the first two clusters maintain the assignment of the bivariate series generated from models 1 and 2, respectively. The difference now lies in the third cluster, which contains the 400 bivariate series obtained from the mixture models 3 and 4. By utilizing three clusters, the ordinary coherence is unable to differentiate between the two mixture models.

In neither of the above cases, whether selecting 3 or 4 clusters, does the ordinary coherence correctly assign the mixture models 3 and 4. In contrast, the quantile coherence enables the placement of each of the 200 bivariate time series in a specific cluster, achieving a perfect separation of the four simulation models.

To provide further detail, the true ordinary coherence for models 3 and 4, which correspond to the mixture models, is simulated. For each model, the average of 5000 raw VAR periodogram matrices is treated as the VAR spectral matrix, from which the true ordinary coherence is derived. In both cases, these models exhibit a peak of coherence around frequency 0.20, as shown in Figure 3. By comparing the results of Figure 3 with those of Figure 1, it can be observed that the difference lies in the fact that model 3 presents a peak of coherence at frequency 0.20, but this occurs at low and intermediate quantile levels. In contrast, model 4, although it presents the peak at the same frequency, is found at intermediate and high quantile levels. Compared to the ordinary coherence, the quantile coherence offers more accurate clustering, as it contains additional information about quantile levels that can be utilized to appropriately assign bivariate series, particularly with mixture models.

Table 2
Stock assignment in hierarchical clustering based on specific quantile regions.

Quantiles	Clusters	Stock Members
Lower	Cluster 1	ADBE ADI AFL AIG ALL AON APD C CSCO DIS DOV EMN IBM JPM LOW MMC MMM MSFT SBUX WFC
	Cluster 2	AAPL ABT ADM AEE AEP AES AMGN AMZN BSX CL CMCSA CVX F GD KMB KO M MCD PEP PFP PG T TGT TM WEN WMT XOM
	Cluster 3	CPB ENB GIS MO NEM
Middle	Cluster 1	ADBE ADI AFL AIG ALL AON APD C CSCO CVX DIS DOV EMN IBM JPM MMC MMM MSFT SBUX WFC XOM
	Cluster 2	AAPL ABT ADM AES AMGN AMZN BSX CL CMCSA F GD KMB KO LOW M MCD PEP PFP PG T TGT TM WMT
	Cluster 3	AEE AEP CPB ENB GIS MO NEM WEN
Upper	Cluster 1	ADBE ADI AFL AIG APD C CMCSA CSCO DIS DOV EMN IBM JPM MMC MMM MSFT WFC
	Cluster 2	AAPL ABT ADM AES ALL AMGN AMZN AON BSX CL CVX F GD KO LOW M MCD PEP PFP PG SBUX T TGT TM WMT XOM
	Cluster 3	AEE AEP CPB ENB GIS KMB MO NEM WEN

Finally, in terms of computational complexity, the most demanding aspect lies in computing the quantile periodogram matrix at each quantile level, as this involves solving the quantile regression problem for each quantile. The quantile periodogram matrix is obtained using the function `qdfit` from the `qfa` package in . Regarding computational time, all experiments and simulations were conducted on a MacBook Pro with a 2.3 GHz 8-Core Intel Core i9 processor. A total of 200 bivariate time series were simulated across four models, as described in Section 3.3. For instance, simulating 200 bivariate time series for Model 3 and computing their quantile coherence takes approximately 3.35 hours.

4. Financial time series clustering

In this section, the goal is to explore the advantages of clustering the time series of stock prices based on their quantile coherence with a benchmark. The objective of this experiment is to determine whether meaningful clusters can be identified among these stocks by considering their co-variability with respect to the benchmark across different quantile regions. A selection of 52 stocks from the S&P 500 (SPX) was made to evaluate the estimation method for quantile coherence and its effectiveness for clustering purposes.

The 52 selected stocks represent different market sectors, including Health Care, Technology, Materials, Consumer Staples, Industrials, Consumer Discretionary, Commodities, Entertainment, Energy, Agricultural Products, Communications Services, Utilities, and Restaurants. Furthermore, the study period spans from 2010 to 2019, a timeframe that is free of large oscillations such as the “Great Recession” and the COVID-19 pandemic.

In this experiment, the time series data consists of the daily log returns of the closing prices of specific companies within the SPX index. Each individual series is represented by a feature vector that incorporates the quantile coherence between the series and the SPX index. This quantile coherence is evaluated at Fourier frequencies ranging from 0 to 1/2. Additionally, the feature vector includes quantile regions, which are subsets of the range from 0.04 to 0.90, totaling 90 quantile levels. To quantify the dissimilarity between these series, a dissimilarity matrix is constructed, based on the pairwise Euclidean distances calculated from the feature vectors derived from quantile coherence.

The proposed approach provides a notable advantage in accurately capturing the combined behavior of log returns with the SPX index. This emphasizes the significance of integrating information about the quantile-dependence characteristics of the data, which holds valuable insights for risk analysis and portfolio construction. In practice, portfolio managers commonly prioritize a fixed quantile level, usually below 10%, as it offers a simplified implementation compared to using a range of quantiles. Specifically, the analysis focuses on three quantile regions: the lower quantile region (quantiles from 4% to 10%), the middle quantile region (quantiles ranging from 40% to 55%), and the upper quantile region (quantiles from 70% to 96%). The results of the cluster assignments obtained from the hierarchical clustering procedure are presented in Table 2, while the corresponding dendrograms can be found in Appendix A.3.

As mentioned in Section 3.3, the optimal number of clusters is determined from the dendrogram using the “elbow rule” (Yuan and Yang, 2019). The within-cluster sum of squares (WSS) is depicted in Figure 4, with the top panel representing lower quantiles, the center panel representing middle quantiles, and the bottom panel representing upper quantiles. In all cases, the optimal number of clusters is found to be 3.

To provide a concise summary of the information contained within each of the three clusters in each quantile region, the centroids of each cluster are calculated by averaging their members. The centroids of the three clusters for each specific quantile region are visualized in Figure 5. The top panel displays the formation of three clusters based on upper quantiles, the center panel illustrates clusters formed using middle quantiles, and the bottom panel showcases the corresponding clusters formed based on lower quantiles.

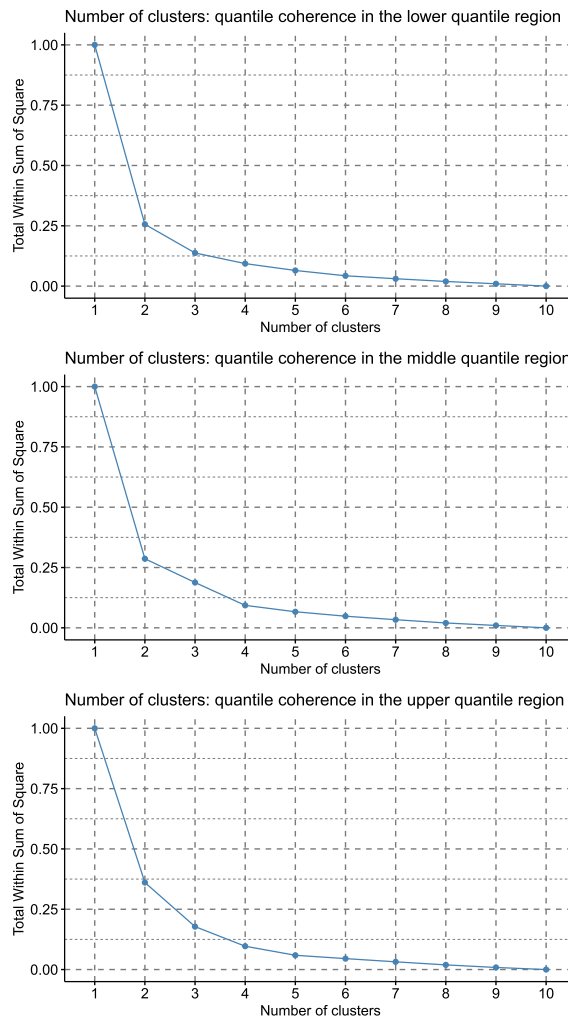


Fig. 4. The total within-cluster sum of squares (WSS) as a function of the number of clusters. (Top) clusters formed using quantile coherence for lower quantile levels. (center) clusters based on quantile coherence for middle quantile levels. (Bottom) clusters based on quantile coherence for upper quantile levels.

It is observed that the overall cluster formation follows a consistent pattern in terms of the distribution of quantile coherence across quantile regions. In particular, Cluster 1 is composed of stocks exhibiting the highest quantile coherence with the SPX. Cluster 2 comprises stocks with intermediate quantile coherence with the SPX, while Cluster 3 consists of stocks with the lowest quantile coherence with the SPX. It is worth noting that for the clusters formed based on the middle quantile regions, the level of quantile coherence is considerably lower compared to the other quantile regions across all clusters.

Cluster 1, depicted in the left column of Figure 5, exhibited high quantile coherence with the SPX index at low frequencies. Interestingly, this cluster also demonstrated significant quantile coherence in the mid-range and high-frequency regions. Notably, among the three clusters, only Cluster 1 displayed such a level of quantile coherence in the middle and high-frequency regions. Further analysis revealed that Cluster 1, based on both lower and upper quantile regions, exhibited the highest level of quantile coherence compared to the middle quantile levels. These findings evidence the importance of quantile dependence in the data.

Cluster 2, illustrated in the center column of Figure 5, consisted of stocks that exhibited a moderate level of quantile coherence with the SPX index in the lower frequency regions within both the lower and upper quantile regions. The quantile coherence in Cluster 2 was stronger than that observed in Cluster 3 but not as high as in Cluster 1. Cluster 2 also contained the largest number of stocks among all quantile regions. Similar to Cluster 3, it lacked significant quantile coherence in other frequency ranges; however, the level of quantile coherence in Cluster 2 was notably higher than in Cluster 3.

Finally, in Cluster 3, displayed in the right column of Figure 5, stocks in this cluster showed a low level of quantile coherence with the SPX index around low-frequency regions in both the lower and upper quantile regions. However, the quantile

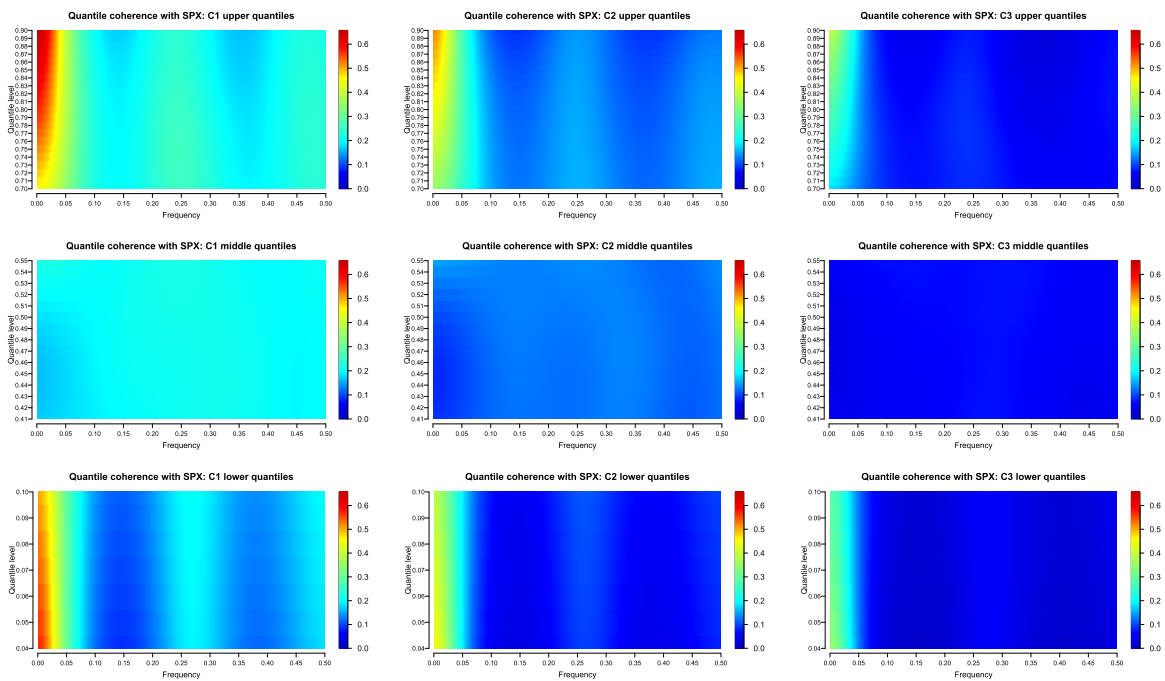


Fig. 5. The quantile coherence spectra for the centroids in each of the 3 clusters with the SPX index. For upper quantiles (first row). For middle quantiles (second row). For lower quantiles (third row).

Table 3

Summary statistics for the beta values obtained for each of the three clusters obtained through quantile coherence.

Quantiles	Clusters	Min	Max	Mean	Sd
Lower	Cluster 1	0.8563	1.5826	1.1079	0.1907
	Cluster 2	0.4821	1.2146	0.8070	0.2368
	Cluster 3	0.4360	0.7903	0.5489	0.1421
Middle	Cluster 1	0.8563	1.5826	1.1420	0.1890
	Cluster 2	0.5070	1.2146	0.8247	0.2392
	Cluster 3	0.4360	0.8427	0.5779	0.1535
Upper	Cluster 1	0.8563	1.5826	1.1410	0.1873
	Cluster 2	0.5194	1.2146	0.8524	0.2179
	Cluster 3	0.4360	0.8427	0.5700	0.1455

coherence observed in Cluster 3 was not as strong as that seen in Clusters 1 and 2. Additionally, no significant quantile coherence activity was observed in other frequency regions. Notably, Cluster 3, based on middle quantiles, demonstrated a very low level of quantile coherence across all frequency regions.

4.1. Capital Asset Pricing Model (CAPM)

The beta coefficient in the Capital Asset Pricing Model (CAPM), a time domain approach, is a standard method of quantifying the systematic risk of equities in the financial industry (Sharpe, 1964; Lintner, 1965; Mossin, 1966). The CAPM methodology distinguishes the stocks that are more sensitive to market movements and those that are less sensitive to such changes. Given that no shocks or other factors caused substantial volatility throughout the period studied, the beta coefficients do not have large values. Stocks with betas above 1 will tend to move with more momentum than the S&P; Stocks with betas less than 1 with less momentum.

The application of the quantile coherence approach reveals clusters that display a certain level of connection with the beta distribution. However, due to their coherence-quantile relationship, the quantile coherence method offers additional insights into their associations with the SPX. As evident from Table 3, we can observe two distinct groups of clusters in terms of the beta distribution across all quantile regions. The first group is Cluster 1 which clearly shows the presence mostly of stocks with high betas (higher than 1). The second group is the one formed with Clusters 2 and 3 which represent stocks with betas on average less than 1. Clusters 2 and 3 are difficult to distinguish from the beta distribution since their beta-value distributions overlap. Using the quantile coherence, these two clusters are distinguished based on their activity connected with specific quantile areas (See Figure 5).

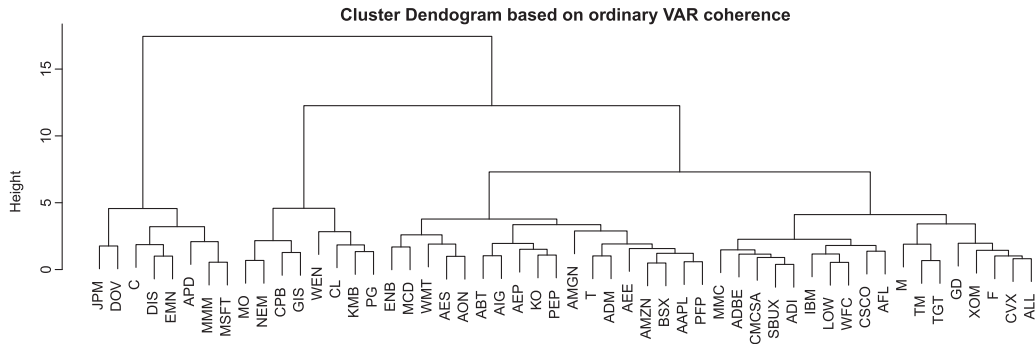


Fig. 6. Dendrogram for the hierarchical clustering of 52 stocks in SPX based on the ordinary coherence with the index.

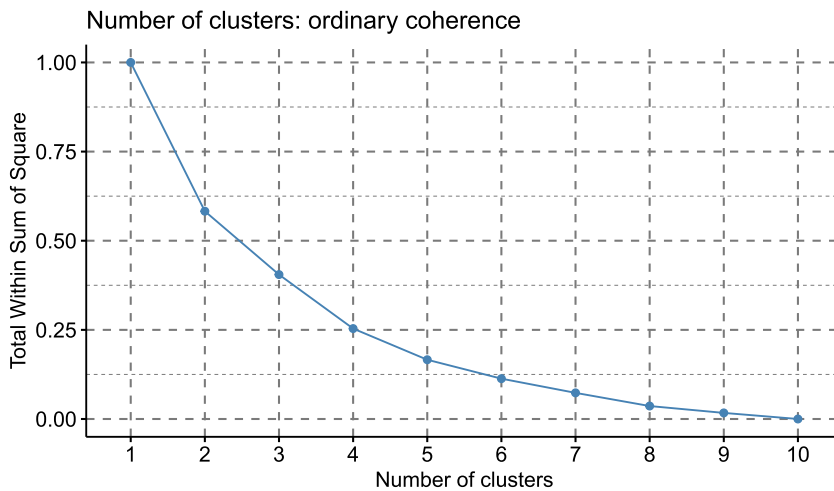


Fig. 7. The total within-cluster sum of Squares (WSS) as a function of the number of clusters.

Table 4
Stock assignment in hierarchical clustering based on ordinary coherence.

Clusters	Stock Members
Cluster 1	APD C DIS DOV EMN JPM MMM MSFT
Cluster 2	AAPL ABT ADBE ADI ADM AEE AEP AES AFL AIG ALL AMGN AMZN AON BSX CMCSA CSCO CVX ENB F GD IBM KO LOW M MCD MMC PEP PFP SBUX T TGT TM WFC WMT XOM
Cluster 3	CL CPB GIS KMB MO NEM PG WEN

4.2. Comparison with ordinary VAR coherence

For comparison, the hierarchical clustering procedure is repeated using the ordinary VAR coherence. The resulting dendrogram is shown in Figure 6. To select the optimal number of clusters in this case, similar to the quantile coherence scenario, the elbow plot is presented in Figure 7. From Figure 7, it is evident that determining an optimal number of clusters is challenging because no clear turning point can be identified. With the sole purpose of making a fair comparison between the quantile coherence and the ordinary coherence in clustering, the same number of clusters is used for the ordinary coherence.

The analysis of the ordinary coherence reveals distinct behaviors within the three clusters, as depicted by the centroids in Figure 8. Cluster 1 exhibits high coherence, Cluster 2 demonstrates moderate coherence, and Cluster 3 displays very low coherence. The stock assignment based on ordinary coherence can be found in Table 4.

The main differences compared to quantile coherence can be observed in Cluster 2, which contains the largest number of stocks. Cluster 1, characterized by quantile coherence, is a more compact cluster that enables a clear distinction between high and moderate quantile coherence, particularly at higher and lower quantile regions. In contrast, when considering ordinary coherence, many stocks initially assigned to Cluster 1 by quantile coherence now belong to Cluster 2.

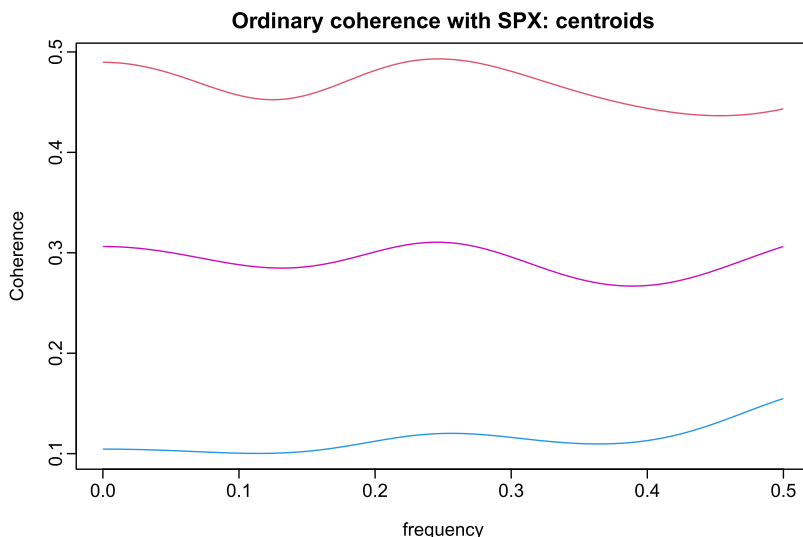


Fig. 8. The ordinary coherence spectra for the centroids in each of the 3 clusters with SPX.

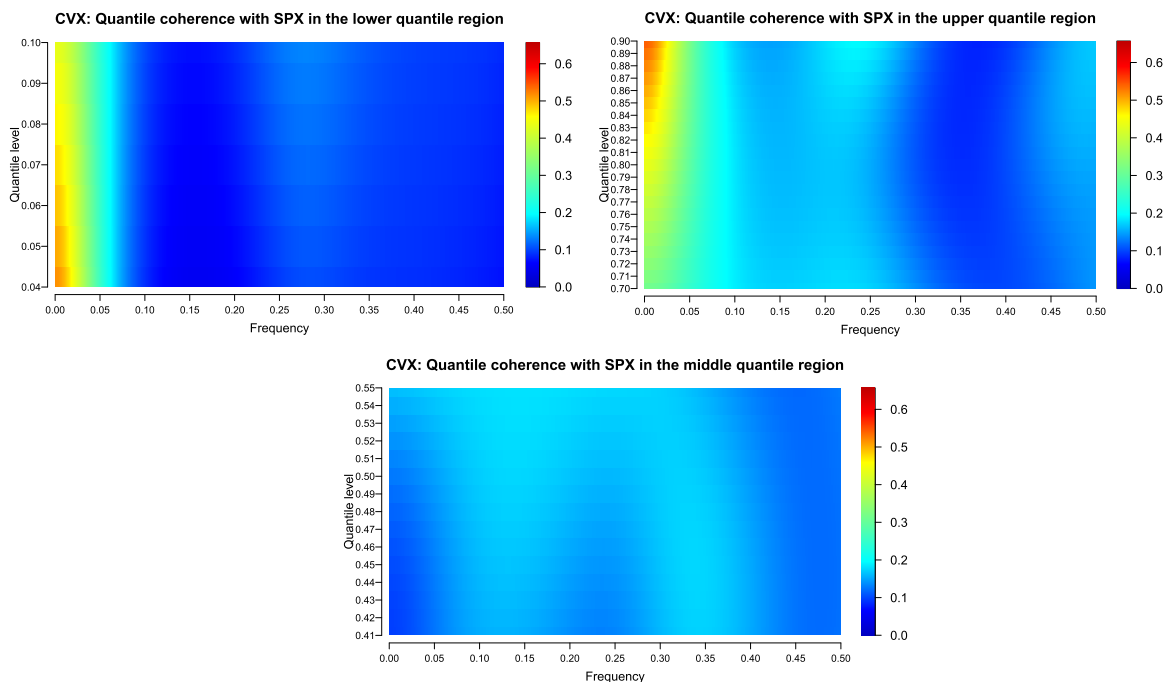


Fig. 9. quantile coherence with SPX for the stock CVX. Top left panel lower quantiles. Top right panel upper quantiles. Bottom panel middle quantiles.

By examining the centroid of Cluster 2 using quantile coherence, specifically at higher quantile regions (refer to Figure 5), it becomes apparent that these stocks are expected to exhibit substantial coherence around the zero frequency region, similar to Cluster 1. Additionally, there is observable activity in the middle and higher frequency regions. However, the level of quantile coherence in the zero-frequency zone is not as pronounced as that of Cluster 1.

Finally, two examples have been chosen to illustrate the enhanced characteristics of hierarchical clustering when utilizing quantile coherence at specific quantile regions. Additionally, an example is included that compares quantile coherence and ordinary coherence during clustering. In Figure 9, an analysis of the quantile coherence for the stock “CVX” in relation to the SPX is provided, focusing on different quantile regions. The top panel displays the quantile coherence at lower and upper quantile levels, while the bottom panel represents the coherence at the middle quantile level.

When clustering “CVX” based on both upper and lower quantile levels, it is assigned to cluster 2, which corresponds to a cluster exhibiting a moderate or middle level of quantile coherence. However, when clustering is performed using the

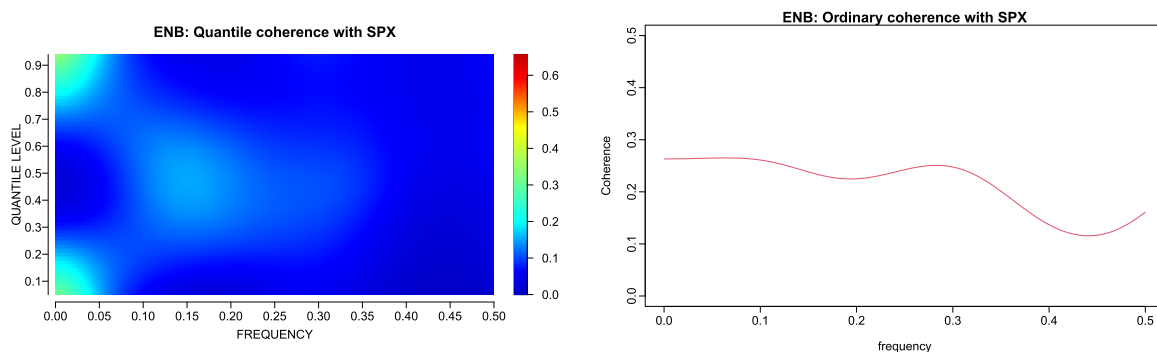


Fig. 10. Left panel: quantile coherence with SPX for the stock ENB. Right panel: ordinary coherence with SPX for the stock ENB.

middle quantile levels, “CVX” is assigned to cluster 1. According to the general behavior, stocks in cluster 1 are expected to demonstrate the highest level of quantile coherence, particularly around the zero frequency region. However, in the case of “CVX”, it is observed that at the middle quantile levels, it does not exhibit a sufficiently high level of quantile coherence to be assigned to cluster 1.

Figure 10 illustrates the comparison between quantile coherence (left panel) and ordinary coherence (right panel) for the stock “ENB” in relation to SPX. It is evident that “ENB” exhibits generally low values of quantile coherence across all quantile levels. Consequently, when considering each of the three quantile regions, “ENB” is assigned to Cluster 3, which is characterized by a low level of quantile coherence. However, when examining the ordinary coherence, “ENB” demonstrates a moderate level of coherence. As a result, it is assigned to Cluster 2 based on the ordinary coherence criterion as it does not consider the quantile information.

5. Discussion

A new semi-parametric method has been developed for estimating the quantile coherence derived from trigonometric quantile regression. The proposed method employs the parametric form of the VAR approximation in conjunction with a nonparametric smoothing technique. The parametric VAR spectrum estimates the multivariate quantile spectral matrix at each quantile. The VAR model is obtained by solving the multivariate Yule-Walker equations formed by the quantile autocovariance function, which is defined as the inverse Fourier transform of quantile periodograms. The AIC criterion, which balances goodness of fit and model complexity, is used to determine the VAR order. The resulting preliminary estimate of the quantile coherence is further smoothed across quantiles by smoothing splines, where the smoothing parameter is selected jointly across frequencies. For selecting the tuning parameter, a \mathcal{K} -fold cross-validation technique is employed to address the correlation found in the estimated quantile coherence across quantiles.

Similar to the quantile periodogram maps previously described in the literature (Li, 2012; 2020), the 2D representation of the quantile coherence provides more information than the ordinary coherence and can be used as images to analyze multivariate time series data.

The results of an application of quantile coherence to financial time series have also been presented. In this application, the daily closing prices of 52 stocks are grouped by their behavior against the SPX index as measured by the quantile coherence. The three clusters are distinguished largely by the coherence patterns in the low-frequency region at high and/or low quantiles. A better cluster formation is obtained by focusing on specific quantile regions, and the quantile-dependent nature enhances cluster formation.

Declaration of competing interest

We hereby certify that there is no conflict of interest.

CRedit authorship contribution statement

Cristian F. Jiménez-Varón: Writing – original draft, Methodology, Investigation, Formal analysis, Data curation, Conceptualization. **Ying Sun:** Writing – review & editing, Supervision, Project administration, Methodology. **Ta-Hsin Li:** Writing – review & editing, Supervision, Project administration, Methodology, Conceptualization.

Appendix A

A1. Multivariate Durbin-Levinson Algorithm and the standard partial autocorrelation function

Whittle (1963) proposed the multivariate version of the Durbin-Levinson recursions, which solve the Yule-Walker equations in (6) with a total of $2p$ inversions of $k \times k$ matrices. (see also proposition 11.4.1 Brockwell and Davis, 1991).

Degerine (1990) proposed a way of defining the partial autocorrelation function for multivariate stationary time series through the canonical analysis of the forward and backward innovations. It is proved that there is a one-to-one correspondence between the resulting PACF and the autocovariance function.

Based on Whittle (1963) and the canonical approach defined by Degerine (1990), the following algorithm is employed to compute the VAR parameters recursively. Given a sequences of covariance matrices $\Gamma(0), \Gamma(1), \dots, \Gamma(p)$,

0. Compute $V_0 = \tilde{V}_0 = \Gamma(0)$ and $\Delta_0 = \Gamma(1)$.

1. For $r = 1, \dots, p$, compute the PACF $\Psi_r = \mathbf{V}_{r-1}^{-1/2} \Delta_{r-1} \tilde{\mathbf{V}}_{r-1}^{-1/2}$.

2. Compute

$$\Phi_{r,r} = \mathbf{V}_{r-1}^{1/2} \Psi_r \tilde{\mathbf{V}}_{r-1}^2$$

$$\tilde{\Phi}_{r,r} = \tilde{\mathbf{V}}_{r-1}^{1/2} \Psi_r^T \mathbf{V}_{r-1}^{1/2}.$$

3. For $p \geq 2$, compute

$$\Phi_{r,r'} = \Phi_{r-1,r'} - \Phi_{r,r} \tilde{\Phi}_{r-1,r-r'}, \quad r' = 1, \dots, r-1$$

$$\tilde{\Phi}_{r,r'} = \tilde{\Phi}_{r-1,r'} - \tilde{\Phi}_{r,r} \Phi_{r-1,r-r'}, \quad r' = 1, \dots, r-1.$$

4. Compute

$$\mathbf{V}_r = \mathbf{V}_{r-1}^{1/2} [\mathbb{I} - \Psi_r \Psi_r^T] \mathbf{V}_{r-1}^{1/2T}$$

$$\tilde{\mathbf{V}}_r = \tilde{\mathbf{V}}_{r-1}^{1/2} [\mathbb{I} - \Psi_r^T \Psi_r] \tilde{\mathbf{V}}_{r-1}^{1/2T}$$

$$\Delta_r = \Gamma(r+1) - \Phi_{r,1} \Gamma(r) - \dots - \Phi_{r,r} \Gamma(1).$$

For the VAR model to be stable, the singular values of the PACF (Ψ_r) must be less than 1 in magnitude. Morf et al. (1978) proposed the orthogonalization procedure based on a Gramm-Schmidt process to compute the PACF and the resulting Durbin-Levinson recursion.

A2. Proof of Equation (8)

By the $2n$ -point inverse discrete Fourier transform, the estimated autocovariance function $\hat{\Gamma}(h) : |h| < n$ can be recovered from Eq. (7), as follows:

Multiplying both sides of Eq. (7) by $e^{i2\pi lk/2n}$ and summing over $l : 0 \leq l \leq 2n-1$,

$$\begin{aligned} (2n)^{-1} \sum_{l=0}^{2n-1} \mathbf{I}_n(\omega_l) e^{i2\pi lk/2n} &= (2n)^{-1} \sum_{l=0}^{2n-1} \sum_{|h|<n} \hat{\Gamma}(h) e^{-i2\pi lk/2n} e^{i2\pi lh/2n} \\ &= (2n)^{-1} \sum_{|h|<n} \hat{\Gamma}(h) \left[\sum_{l=0}^{2n-1} e^{i2\pi (h-k)l/2n} \right], \end{aligned}$$

with $h = k$,

$$= \hat{\Gamma}(h), \quad h = 0, 1, \dots, n-1.$$

A3. Hierarchical clustering based on specific quantile regions

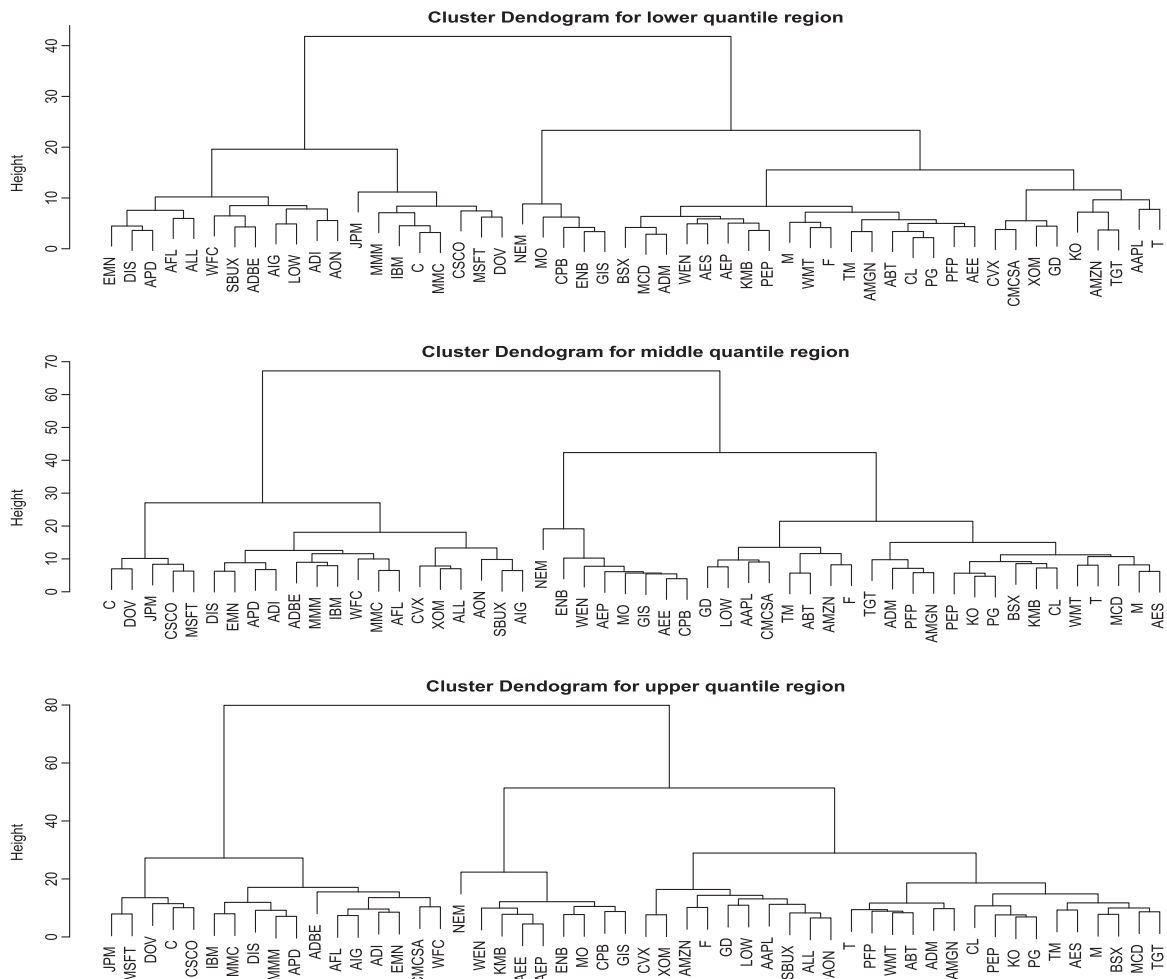


Fig. A1. Dendrogram for the hierarchical clustering of 52 stocks in SPX based on the quantile coherence of their daily log returns with the index SPX. The top panel displays clusters formed using quantile coherence for lower quantile levels. The center panel depicts clusters based on quantile coherence for middle quantile levels. The bottom panel represents clusters based on quantile coherence for upper quantile levels.

References

- Akaike, H., 1969. Power spectrum estimation through autoregressive model fitting. *Annals of the Institute of Statistical Mathematics* 21 (1), 407–419.
- Akaike, H., 1974. A new look at the statistical model identification. *IEEE Transactions on Automatic Control* 19 (6), 716–723. doi:10.1109/TAC.1974.1100705.
- Altman, N.S., 1990. Kernel smoothing of data with correlated errors. *Journal of the American Statistical Association* 85 (411), 749–759.
- Baruník, J., Kley, T., 2019. Quantile coherency: A general measure for dependence between cyclical economic variables. *Econometrics Journal* 22, 131–152. doi:10.1093/ectj/utz002.
- Baruník, J., Nevrla, M., 2022. Quantile Spectral Beta: A Tale of Tail Risks, Investment Horizons, and Asset Prices. *Journal of Financial Econometrics* 21 (5), 1590–1646.
- Bishnoi, S.K., Ravishanar, N., 2018. Clustering time series based on quantile periodogram. Technical Report. University of Connecticut, Department of Statistics.
- Brockwell, P., Davis, R., 1991. *Time Series: Theory and Methods*. Springer. https://books.google.com.sa/books?id=_DcYu_EhVzUC
- Burg, J., 1975. Maximum Entropy Spectral Analysis. Stanford University. https://books.google.com.sa/books?id=Xug_AAAAIAAJ
- Capon, J., 1983. *Maximum-likelihood spectral estimation*. Springer Berlin Heidelberg, Berlin, Heidelberg, pp. 155–179.
- Chen, T., Sun, Y., Li, T.-H., 2021. A semi-parametric estimation method for the quantile spectrum with an application to earthquake classification using convolutional neural network. *Computational Statistics & Data Analysis* 154, 107069. doi:10.1016/j.csda.2020.107069.
- Choi, B., 1993. Multivariate maximum entropy spectrum. *Journal of Multivariate Analysis* 46 (1), 56–60.
- Degerine, S., 1990. Canonical partial autocorrelation function of a multivariate time series. *The Annals of Statistics* 18 (2), 961–971.
- Dette, H., Hallin, M., Kley, T., Volgushev, S., 2015. Of copulas, quantiles, ranks and spectra: An L_1 -approach to spectral analysis. *Bernoulli* 21 (2), 781–831. doi:10.3150/13-BEJ587.

- Euán, C., Sun, Y., Ombao, H., 2019. Coherence-based time series clustering for statistical inference and visualization of brain connectivity. *The Annals of Applied Statistics* 13 (2), 990–1015. doi:10.1214/18-AOAS1225.
- Hastie, T., Tibshirani, R., Friedman, J., 2017. *The Elements of Statistical Learning*, second edition Springer Series in Statistics. <http://www.springer.com/series/692>
- Hurvich, C.M., Tsai, C.-L., 1989. Regression and time series model selection in small samples. *Biometrika* 76 (2), 297–307.
- Kley, T., 2016. Quantile-based spectral analysis in an object-oriented framework and a reference implementation in R: The quantspec package. *Journal of Statistical Software* 70 (3), 1–27.
- Kley, T., Volgushev, S., Dettes, H., Hallin, M., 2016. Quantile spectral processes: Asymptotic analysis and inference. *Bernoulli* 22 (3), 1770–1807.
- Li, T.-H., 2008. Laplace periodogram for time series analysis. *Journal of the American Statistical Association* 103, 757–768. doi:10.1198/016214508000000265.
- Li, T.-H., 2012. Quantile periodograms. *Journal of the American Statistical Association* 107, 765–776. doi:10.1080/01621459.2012.682815.
- Li, T.-H., 2013. *Time series with mixed spectra*. CRC Press.
- Li, T.-H., 2020. From zero crossings to quantile-frequency analysis of time series with an application to nondestructive evaluation. *Applied Stochastic Models in Business and Industry* 36, 1111–1130. doi:10.1002/asmb.2499.
- Li, T.-H., 2021. Quantile-frequency analysis and spectral measures for diagnostic checks of time series with nonlinear dynamics. *Journal of the Royal Statistical Society: Series C (Applied Statistics)* 70 (2), 270–290.
- Lintner, J., 1965. Security prices, risk, and maximal gains from diversification. *The Journal of Finance* 20 (4), 587–615.
- Lütkepohl, H., 2005. *New Introduction to Multiple Time Series Analysis*. Springer.
- Maadooliat, M., Sun, Y., Chen, T., 2018. Nonparametric collective spectral density estimation with an application to clustering the brain signals. *Statistics in Medicine* 37 (30), 4789–4806.
- Morf, M., Vieira, A., Kailath, T., 1978. Covariance characterization by partial autocorrelation matrices. *The Annals of Statistics* 6 (3), 643–648.
- Mossin, J., 1966. Equilibrium in a capital asset market. *Econometrica* 34 (4), 768–783.
- Newton, H.J., Pagano, M., 1981. On the stationarity of multiple autoregressive approximants: theory and algorithms. *Journal of Statistical Computation and Simulation* 13 (3–4), 195–208.
- Parzen, E., 1982. Maximum entropy interpretation of autoregressive spectral densities. *Statistics & Probability Letters* 1 (1), 7–11.
- Parzen, E., 1983. Autoregressive spectral estimation. In: *Handbook of Statistics*, Vol. 3. Elsevier, pp. 221–247.
- Pawitan, Y., O'Sullivan, F., 1994. Nonparametric spectral density estimation using penalized whittle likelihood. Source: *Journal of the American Statistical Association* 89, 600–610.
- Priestley, M.B., 1981. *Spectral analysis and time series*. Academic Press Inc.
- Schwarz, G., 1978. Estimating the dimension of a model. *The Annals of Statistics* 6 (2), 461–464.
- Sharpe, W.F., 1964. Capital asset prices: A theory of market equilibrium under conditions of risk. *The Journal of Finance* 19 (3), 425–442.
- Shumway, R.H., Stoffer, D.S., 2017. *Time Series Analysis and Its Applications With R Examples*, fourth edition Springer Texts in Statistics. <http://www.springer.com/series/417>
- Wahba, G., 1980. Automatic smoothing of the log periodogram. Source: *Journal of the American Statistical Association* 75, 122–132.
- Wang, Y., 1998. Smoothing spline models with correlated random errors. *Journal of the American Statistical Association* 93 (441), 341–348.
- Whittle, P., 1963. On the fitting of multivariate autoregressions, and the approximate canonical factorization of a spectral density matrix. *Biometrika* 50 (1/2), 129–134.
- Wiener, N., Masani, P., 1957. The prediction theory of multivariate stochastic processes. *Acta Mathematica* 98 (1), 111–150.
- Wiener, N., Masani, P., 1958. The prediction theory of multivariate stochastic processes, II. *Acta Mathematica* 99 (1), 93–137.
- Wise, G., Traganitis, A., Thomas, J., 1977. The effect of a memoryless nonlinearity on the spectrum of a random process. *IEEE Transactions on Information Theory* 23 (1), 84–89. doi:10.1109/IT.1977.1055658.
- Yuan, C., Yang, H., 2019. Research on k-value selection method of k-means clustering algorithm. *J 2* (2), 226–235.